# Lip Leakage Flow Simulation for the Gravity Probe B Gas Spinup Using PSiCM

Leonardo Dagum[1]

Report RNR-91-010, March 5, 1991

NAS Applied Research Laboratory
NASA Ames Research Center, Mail Stop T-045-1
Moffett Field, CA 94035

March 5, 1991

**Abstract**

The lip leakage flow for the Gravity Probe B (GP-B) gas spinup system is investigated using a two dimensional particle simulation on the Connection Machine (PSiCM). Particle simulation is employed because the flow conditions are in the transition regime between continuum and free molecule where particle methods are of greatest use. The dominant flow is Couette in nature and the simulation is first validated through comparison to theoretical results for Couette flow in the transitions regime. A GP-B type geometry is then simulated and results are presented for two conditions, those corresponding to near the inlet and near the outlet of the spinup channel. Comparison to experiment is not made because experimental data is not yet available.

[1]The author is an employee of Computer Sciences Corporation.

## 1 Introduction

Gravity Probe B (GP-B) is an effort to experimentally validate the general theory of relativity. The basis of the experiment is to measure any coupling of earth's gravitational tensor with the angular momentum of 4 spherical gyroscopes placed in a drag free orbit about the earth. The experiment has been reviewed in [1] and will not be discussed here. The aspect of the experiment which is of concern in this work is the spinup system. One of the long standing challenges of the GP-B effort has been to design a system which can spin the rotors of the gyroscopes to 170 Hz at temperatures below 9° Kelvin (the transition temperature of the superconducting niobium film coating on the gyroscopes).

The proposed spinup system is described by Xiao [2]. The spinup system is constrained to fit into the current design of the experiment and it is required that

1. The system operate at temperatures below 9° Kelvin.
2. The gas leakage rate be less than $70\mu$g/sec
3. The gas flow rate be less than 2 mg/sec with an exhaust pressure of 0.35 torr or higher.
4. The system should operate at a background pressure as high as 0.4 millitorr.

The difficulty arises in meeting the second constraint. This constraint is fixed by the size of the vacuum pump which will be used to evacuate the system once the gyroscopes have reached the operating spin speed.

The system consists of a single spinup channel and a sonic nozzle (see figure 1). The spinup channel is surrounded by a larger auxiliary channel. The channels are cut from the inner side of the gyroscope housing, and the gyroscope surface acts as the fourth wall. Figure 1 consists of a cross-sectional and a plan view of the gyroscope and gyroscope housing around the spinup and auxiliary channels. The top figure is the cross-sectional view. The hashed line represents the gyroscope. The bottom figure is the plan view. The shaded areas represent in the auxiliary channel represent sinks in the auxiliary channel flow. These are connections to the pumping system; the arrows indicate the direction of flow. The shaded area in the spinup channel represents a source in the spinup channel flow. This is the outlet of a nozzle which impinges Helium on the gyroscope causing it to rotate in the direction of the wide arrow in the figure. The arrows from the spinup channel to the auxiliary channel indicate the direction of the leakage flow, that is, the flow which leaks from the spinup channel through the channel lip.

The flow in the gyroscope spinup system can be divided into 4 sections: flow in the spinup channel, flow over the channel lip, flow in the auxiliary channel and flow in the rest of the housing. The flow in the spinup channel is in the continuum regime, and the flow in the auxiliary channel and in the rest of the housing is in the free molecule regime. Therefore these sections of the analysis can be carried out without great difficulty by applying the well established equations governing flow in those regimes. However, the flow over the channel lip is in the *transition regime* between continuum and free molecule flow. This flow is best handled through a particle simulation. Because of the very close spacing between the housing and the gyroscope, the shear stress on any gas flowing through this gap will be much higher than anywhere else in the gyroscope. It is expected that the lip leakage flow will contribute up to 80% of the parasitic drag in the spinup. It is very important to have a good model of this flow since excessive parasitic drag must be overcome by a greater nozzle flow rate which is constrained by the pumping system.

PSiCM is a highly optimized two dimensional particle simulation implemented on the Connection Machine at NAS [5]. The work being carried out at NAS as part of the GP-B effort involves adapting PSiCM to simulate the lip leakage flow in the gyroscope spinup system. A two step approach has been undertaken. The first step has been to properly model the particle/surface interaction at the conditions of interest. For this purpose, PSiCM was set up to simulate a Couette flow at the very low temperatures under consideration. This afforded a useful comparison of the simulation to theory, since Couette flow is well understood throughout the transition regime and approximate analytical models do exist (for example, see Vincenti and Kruger [3]). Once the Couette flow problem was properly handled by the simulation, the channel lip geometry was simulated and drag and leakage rate data collected. Currently, Yueming Xiao of Stanford is carrying out an experimental investigation of the gas spinup system and a comparison of simulation results with experimental results will be possible. It is hoped that simulation results will be available before full scale experiments are carried out (now scheduled for March 1991) thus providing a better understanding of the flow and aiding in the design of the experiment.

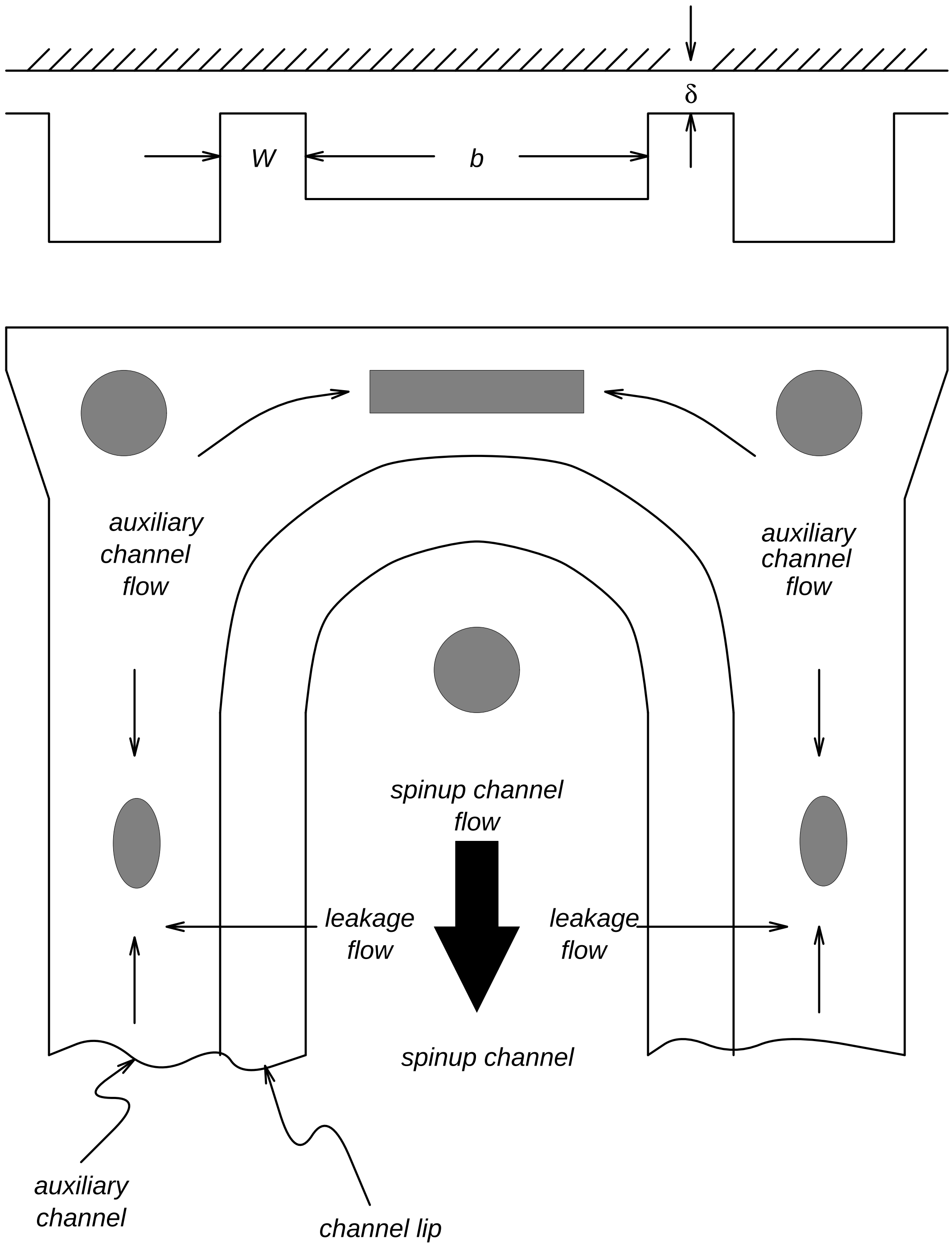


Figure 1: Spinup channel and gyroscope.

## 2 Particle/Surface Interaction Model

The particle/surface interaction model used for these simulations is the perfectly diffuse reflection model [4] first proposed by Maxwell in 1879. In a perfectly diffuse reflection, a particle striking the surface is assumed to remain trapped on the surface for sufficient time to lose all relation to its pre–interaction state. The reflected direction of a particle is completely independent of its incident direction and the probability of a particular reflected direction is proportional to the cosine of the reflection angle (measured from the surface normal). Furthermore, the reflected gas is assumed to have acquired a temperature equal to that of the surface. In the simulation, a reflected particle's tangential velocity components are sampled from a Maxwellian distribution at the surface temperature, and the normal velocity component is sampled from the distribution function for flux across a plane. This is equivalent to treating the element of surface area as a transparent plane with a Maxwellian gas at rest and at the surface temperature behind it. The reflected particles move from this gas into the flow through the transparent plane.

The Maxwellian distribution, $f$, is given by [3]

$$f(C_i) = \left(\frac{m}{2\pi kT}\right)^{3/2} exp\left[-\frac{m}{2kT}(C_1^2 + C_2^2 + C_3^2)\right] \tag{1}$$

where $C_i$ is the $i^{th}$ component of velocity, $m$ is the mass of the molecule, $k$ is Boltzmann's constant and $T$ is the temperature. This distribution is used to sample velocity components tangential to the surface. Clearly there is no bias on the particles in the tangential direction and the tangential velocity distribution of particles crossing a plane in an equilibrium gas must be given by the Maxwellian distribution. In the normal direction, however, the Maxwellian distribution cannot be used since not all particles in the equilibrium gas are equally likely to cross the plane. The normal velocity distribution of particles crossing a plane can be deduced by considering the number flux across the plane. The flux across a plane of any quantity $Q$ is given by (cf. reference [4])

$$n < QC_n > \tag{2}$$

where $C_n$ is the velocity component normal to the plane and the angle brackets are used to denote a mean quantity. For an equilibrium gas with velocity distribution $f$, the number flux is given by setting $Q = 1$ and integrating

$$n \int_{-\infty}^{\infty} \int_{-\infty}^{\infty} \int_{0}^{\infty} C_n f dC_n dC_t \qquad (3)$$

where $C_t$ is the tangential velocity component. It follows that the normal velocity distribution, $f_n$, for particles crossing a plane must be given by the integrand of 3, or

$$f_n(C_n) = C_n f(C_n). \qquad (4)$$

## 3 Model Validation – Couette Flow Results

As mentioned above, a Couette flow simulation was carried out in order to validate the models used. Couette flow appeared as a very appropriate model problem for several reasons. Most importantly, approximate analytical solutions exist (see [3]) and these can be used for comparison with the simulation results. As well, Couette flow essentially is a degenerate case of the lip leakage flow obtained when there exists equal pressure in the spinup channel and the auxiliary channel. Therefore by correctly simulating Couette flow at the conditions of interest for the GP-B experiment one can feel confident in the simulation results for the lip leakage flow. In this way the Couette flow problem is used to validate the particle/surface interaction model, the geometry of the simulation, and the chosen particle interaction potential.

Although Couette flow is one dimensional in nature, the Couette flow simulation was carried out in a two dimensional geometry of about the same dimensions as was later used for the lip leakage simulation. This was useful in determining appropriate parameters for running the lip leakage simulation. The Couette geometry used a rectangular cell network of dimensions $250 \times 32$ and was initialized with 16 particles per cell (see figure 2). The upper boundary was stationary and assumed isothermal at the initial gas temperature (which corresponded to $7°$ K). The lower boundary was also isothermal and at the initial gas temperature but moving in the $z$ direction at a fixed velocity $w_{gyro}$. In order to speed up the transient, the particles were initialized with a linear gradient from 0 to $w_{gyro}$ in the $z$ velocity component. This was especially useful at very small Knudsen numbers where, with a subsonic Mach number, the velocity diffusion from the moving surface can be exceedingly slow.

On a typical run, 2900 timesteps were carried out to reach steady state. The particles were then cloned twice and 100 timesteps were carried out to eliminate any statistical dependencies from the cloning. Following this,

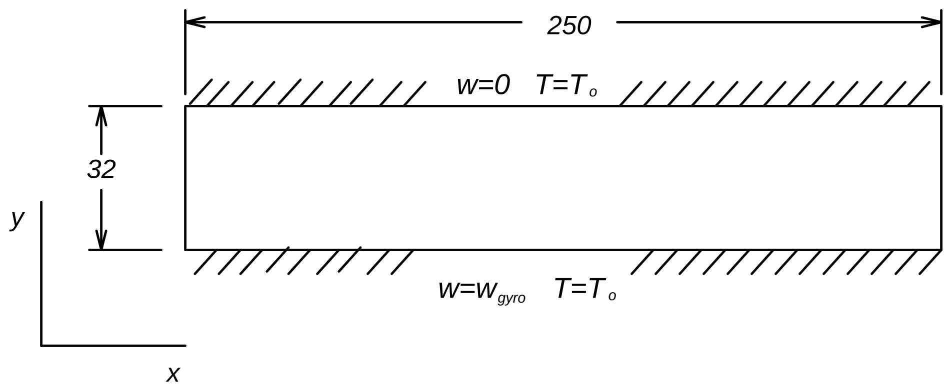


Figure 2: Geometry for Couette flow simulation.

the simulation was run for 1500 timesteps with sampling on every timestep (corresponding to about $10^5$ samples per cell) to generate a solution. Figure 3 presents the drag on the moving wall (normalized by the drag in the free molecule limit) as a function of the Knudsen number. The Knudsen number for these flows was defined as

$$K_n = \lambda_0/\delta \tag{5}$$

where $\lambda_0$ is the initial (undisturbed gas) mean free path and $\delta$ is the width between the two plates. Results were obtained for Maxwell, hard sphere, and inverse $9^{th}$ power law interaction potentials. The wall Mach number was 0.333 and the Knudsen number ranged from 0.031 to 10.0. The simulation results are shown compared to Lees' theoretical results as given in [3] (the solid curve in the figure). Both the inverse $9^{th}$ and the hard sphere potentials give good fits to Lees' solution, however, the hard sphere potential gives a better fit at the lower Knudsen numbers and this potential was chosen for the GP-B simulations.

Figure 4 shows the velocity profiles (normalized by $w_{gyro}$) for the hard sphere interaction potential with moving wall Mach number of 0.333 and Knudsen numbers ranging from 0.031 to 10.0. The results were generated by ensemble averaging across the 250 columns of cells in the two dimensional geometry. The profiles are all relatively flat as would be expected for such low Mach numbers. Furthermore, the intersection point for all the profiles is at $w/w_{gyro} = 0.5$ and $y/\delta = 0.5$, again as would be expected.

Figure 5 shows the shear stress profiles normalized by the free molecule value. These results again are for the hard sphere interaction potential and moving wall Mach number of 0.333. It is encouraging to see such flat profiles especially near the boundaries. Because the shear stress is a second moment of the velocity distribution, it is particularly susceptible to small disturbances in the gas. The absence of disturbances near the boundaries indicates that they are being handled correctly correctly by the simulation. The shear stress profile at the lowest Knudsen number considered ($K_n$ = 0.031) is not as flat as would be desired. At these conditions (i.e. near continuum and subsonic) it becomes very difficult to generate good solutions because the velocity distributions defined by the particles are very noisy. At this point one is better served by considering continuum methods of solution.

## 4 GP-B Simulation – Geometry and Relevant Parameters

The GP-B geometry was approximated as shown in figure 6. The spinup channel is modelled by the rectangular, $80 \times 32$, chamber in the left of the figure. The channel lip is modelled by the $350 \times 16$ chamber to the right of this, and the auxiliary channel is modelled by the $80 \times 32$ chamber at the right end of the figure. The aspect ratio of the channel lip is 21.9; this value was chosen to correspond with the experimental set up which is to use a gap width of 0.023mm and a gap length of 0.50mm. The hashed boundaries are diffusely reflecting and at a fixed temperature $T_\circ$. The lower boundary is allowed to move in the $z$-direction at velocity $w_{gyro}$ while the upper boundary is fixed. The boundary at the right hand end of the figure is an exit boundary. All particles crossing that boundary are removed from the flow. The remaining six boundaries are specularly reflecting.

The flow of interest for these simulations is the lip leakage flow (see figure 1). Particles were initialized with temperature $T_\circ$, pressure $p_\circ$, and initial flow velocity $w_\circ$ in the $z$-direction. The flow was initialized only in the spinup and lip chambers, each with an initial number density, $n_\circ$, of 13 particles per cell. The auxiliary chamber was evacuated. The simulation was run for 3900 time steps to clear the transient then particles were cloned three times thus increasing the total number of particles by a factor of 8. The simulation was run for another 100 time steps before time averaging began. Time averaging was carried out for 1500 time steps with samples collected on every time step. Typically, there were some $7.5 \times 10^5$ particles in the flow for the time averaging phase.

During the calculation, new particles were introduced in the spinup chamber at the initial conditions and at a mean fill rate of $n_\circ/10$ particles per time step. The fill rate was an input value for these simulations.

| run | $a_\circ$ (cells/timestep) | $w_\circ$ (cells/timestep) | $M_{z_\circ}$ | $\lambda_\circ$ (cells) | $T_w/T_\circ$ | $w_{gyro}$ (cells/timestep) |
|---|---|---|---|---|---|---|
| 1 | 0.15 | 0.05 | 0.33 | 1.0 | 1.0 | 0.00 |
| 2 | 0.15 | 0.05 | 0.33 | 1.0 | 1.0 | 0.005 |
| 3 | 0.15 | 0.05 | 0.33 | 1.0 | 1.0 | 0.01 |
| 4 | 0.15 | 0.05 | 0.33 | 1.0 | 1.0 | 0.02 |
| 5 | 0.15 | 0.05 | 0.33 | 1.0 | 1.0 | 0.03 |
| 6 | 0.15 | 0.05 | 0.33 | 1.0 | 1.0 | 0.04 |
| 7 | 0.15 | 0.05 | 0.33 | 1.0 | 1.0 | 0.05 |

Table 1: Relevant parameters for simulations corresponding to conditions near the inlet of spinup channel.

Since the conditions for the simulations all lead to choked flow, the results were fairly insensitive to the fill rate.

Two sets of runs were carried out; the relevant parameters are listed in tables 1 and 2. The first set of runs corresponded to conditions near the inlet of the spinup channel. The second set of runs corresponded to conditions near the outlet of the spinup channel. The values are listed in simulation units where $a_\circ$ is the initial speed of sound, $w_\circ$ is the initial bulk velocity in the $z$-direction, $M_{z_\circ}$ is the initial Mach number in the $z$-direction, $T_w$ is the diffuse reflecting wall temperature, and $T_\circ$ is the initial gas temperature. Initial conditions generally are equivalent to the conditions in the spinup channel throughout the calculation, therefore the subscript "$_\circ$" also corresponds to the spinup channel conditions. In both sets of runs, the gas temperature and pressure were held fixed while the gyroscope's velocity was varied. Drag on the gyroscope was measured only in the channel lip and auxiliary channel.

Table 3 lists the assumed conditions for the inlet and outlet of the spinup channel. These values may be used to convert from simulation units to physical units. Note that for the near inlet conditions, the geometry of figure 6 leads to a channel lip length ($x$-direction) of 0.38mm rather than the 0.50mm expected for the experiment. The simulation cannot be run with mean free paths smaller than 1.0 cells, consequently it was not possible to exactly simulate the near inlet conditions. To first order, one can correct for this in the drag measurements by scaling the drag results with a factor of 0.50/0.38.

| run | $a_\circ$ (cells/timestep) | $w_\circ$ (cells/timestep) | $M_{z_\circ}$ | $\lambda_\circ$ (cells) | $T_w/T_\circ$ | $w_{gyro}$ (cells/timestep) |
|---|---|---|---|---|---|---|
| 1 | 0.15 | 0.075 | 0.5 | 1.6 | 1.0 | 0.00 |
| 2 | 0.15 | 0.075 | 0.5 | 1.6 | 1.0 | 0.01 |
| 3 | 0.15 | 0.075 | 0.5 | 1.6 | 1.0 | 0.02 |
| 4 | 0.15 | 0.075 | 0.5 | 1.6 | 1.0 | 0.03 |
| 5 | 0.15 | 0.075 | 0.5 | 1.6 | 1.0 | 0.04 |
| 6 | 0.15 | 0.075 | 0.5 | 1.6 | 1.0 | 0.05 |

Table 2: Relevant parameters for simulations corresponding to conditions near the outlet of spinup channel.

| | $T_\circ$ ($^\circ$ K) | $T_w$ ($^\circ$ K) | $M_z$ | $P_\circ$ (Pa) | $\lambda_\circ$ ($\mu$m) |
|---|---|---|---|---|---|
| near inlet | 7.0 | 7.0 | 0.33 | 227 | 1.1 |
| near outlet | 7.0 | 7.0 | 0.50 | 107 | 2.0 |

Table 3: Experimental conditions near the inlet and the outlet of the spinup channel

## 5 GP-B Simulation – Results

Figure 7 presents the results for the drag on the gyroscope in the channel lip and auxiliary channel sections as a function of the gyroscope velocity. Results for the near inlet conditions are indicated by an 'o' and results for near outlet conditions are indicated by an 'x'. The drag is normalized by unit depth (i.e. in the $z$-direction). As expected, the drag increases linearly with the gyroscope velocity. The observed deviations from linearity are attributable to the statistical nature of solutions generated by a particle simulation. This is especially noticeable in the near inlet calculations where the Mach number in the spinup channel was only 0.33 making it difficult to obtain a clean solution. Furthermore, as described in the previous section, the equivalent length ($x$-direction) of the channel lip was shorter for the near inlet simulations and this was accounted for as described in that section.

A least squares fit was made of the data points and the resulting lines are shown in the figure. Note that the lines do not pass through the origin. For a Couette flow one would expect the drag to go to zero for a zero plate velocity. This is not the case for the GP-B geometry because the the plates are not infinite (in the $x$-direction). With plates of finite length one has to consider the effects of the velocity profiles at either end of the plates. In the present case, at the spinup side gas is introduced with some bulk velocity in the $z$-direction and the gas that leaks through the channel lip has some momentum in the $z$-direction. Consequently, when the gyroscope is stationary, there is momentum imparted to it by the leakage gas in the channel lip section. This effect should become more pronounced for a shorter length channel lip.

Figure 8 presents a typical result for the shear stress between the $y$ and $z$ components of velocity. This result is taken from run 6 of table 2 (the near outlet conditions). The leakage flow is from left to right and the gyroscope surface corresponds to the near boundary in the figure. The figure is meant only to give qualitative information about the flow. The height of each mesh point corresponds to the mean of the shear stress of four neighbouring cells. This averaging was performed to smooth out the figure.

Two things may be learnt from figure 8. First, it is evident that the greatest shear stress occurs in the channel lip section. Since the drag on the gyroscope is proportional to the shear stress at the gyroscope boundary, one can expect that the channel lip will be the greatest source of drag in the spinup process. Second, the shear stress across the width ($y$-direction) of the channel lip is fairly uniform except near the spinup channel. Therefore, using the average of the 16 rows of cells in the channel lip, one can quantitatively study the shear stress in the flow.

Figure 9 presents the shear stress through the channel lip for the near inlet conditions. Each point in the curves represents the average of 160 cells taken as follows: the 16 rows of cells in the channel lip were averaged, then each 10 consecutive values in this result were averaged. In other words,

$$< \tau >_k = \sum_{j=k-9}^{j=k} \sum_{i=0}^{i=15} \tau_{ij} \tag{6}$$

where $i$ is the row, $j$ is the column, $\tau$ is the shear stress between the $y$ and $z$ components of velocity, and $< \tau >$ is the smoothed value. Physical units are used in the figure. The channel lip begins at $x = 0.87 \times 10^{-4}$m and ends at $x = 4.71 \times 10^{-4}$m. The highest curve corresponds to run 7 of table 1, where $w_g/w_\circ = 1.0$, and the lowest curve corresponds to run 1 of table 1, where $w_g/w_\circ = 0.0$.

It is of interest to note that since the shear stress is relatively constant throughout the channel lip, the drag from the channel lip will grow in direct proportion to the length ($x$-direction) of the lip. This supports the use of the correction factor, 0.50/0.38, in computing the drag from the near inlet simulations.

Figure 10 presents the shear stress through the channel lip for the near outlet conditions. This figure was created using the same averaging as in figure 9. The channel lip begins at $x = 1.16 \times 10^{-4}$m and ends at $x = 6.25 \times 10^{-4}$m. The highest curve corresponds to run 6 of table 2, where $w_g/w_\circ = 0.67$, and the lowest curve corresponds to run 1 of table 2, where $w_g/w_\circ = 0.0$. The form of these curves is the same as in figure 9, however the higher Mach number in the spinup channel leads to a greater shear stress through the channel lip and therefore a correspondingly greater drag (see figure 7).

Of interest for the GP-B experiment is the leakage rate of the spinup system. As was mentioned above, the conditions for the simulation resulted in a choked flow so the leakage rate (that is, the rate at which particles exit the simulation) was constant for both the near inlet and near outlet conditions. For near inlet conditions the mean leakage rate was 23.7 particles per cell per unit depth. In physical units this works out to 4.05 mg/s per meter depth. Since the actual spinup channel is measure 2.327 cm this would mean a leakage rate of 0.096 mg/s per side or 0.192 mg/s in total. For the near outlet conditions, the simulation mean leakage rate was 23.0 particles per cell per unit depth which, through a similar calculation, converts to a total leakage rate of 0.116 mg/s. The difference between the two results is due, in part, to the different lengths of gap in the two cases. Recall that the near inlet conditions simulated a gap of length 0.38 mm whereas the near outlet conditions simulated a gap of length 0.50 mm. The shorter gap allows a greater leakage rate but also produces less drag. Clearly there is a design tradeoff in the gap length which should be addressed.

The calculations presented here were carried out on the Connection Machine Model CM2 at the National Aerodynamic Simulation (NAS) facility in NASA Ames. The machine consists of 32768 bit serial processors and 1024 64-bit Weitek floating point units. Each bit serial processor has 128 kB of memory and the machine in total has 4 GB of memory. The calculations were run using only half of the available processors with which each calculation on the GP-B geometry required about 90 minutes to complete. For comparison with other calculations the normalized units of time per particle per timestep is often used. This value was $3.3\mu$s/particle/timestep during the transient phase and $2.8\mu$s/particle/timestep during the time averaging phase. The lower performance during the transient phase is due to the lower virtual processor ratio used in that part of the calculation (this is discussed in [5]). Using the whole machine (i.e. all 32768 processors) would approximately halve these times. By comparison, one processor of the Cray YMP running the fully vectorized equivalent of PSiCM typically obtains 1.0$\mu$s/particle/timestep and is about 40% faster than the CM2 for these calculations.

## 6 Further Research

The work presented in this paper is primarily a validation of the particle simulation method for simulating the lip leakage flow in the GP-B experiment. Even as such it it is severely limited by the lack of corresponding experimental results and therefore can only be viewed as preliminary in nature. The work does succeed in validating the method against known theoretical results for Couette flow, which is expected to be dominant in the experiment, and presents results from the simulation of a GP-B type geometry at the conditions expected for the experiment. Further work should proceed when experimental data become available. At that point, comparison between simulation and experiment will be possible and lead to a more complete validation of the method. Succeeding this the simulation should be used to study the effect of the spinup channel geometry on the leakage flow (an issue which is left completely untouched in the present work) and the tradeoff between gap length and leakage rate should be assessed.

## Acknowledgments

The author would like to gratefully acknowledge David Bailey, John Krystynak and Horst Simon for their insightful comments on reviewing the manuscript.

## References

[1 ] *Science*, November 1990.

[2 ] Xiao, Yeuming, *A Low Pressure Gas Spinup System for GP-B Gyroscope*, GP-B Tech Report, S0136, May 1990.

[3 ] Vincenti, W.G., Kruger, C.H., *Introduction fo Physical Gas Dynamics*, Robert E. Krieger Publishing Co. 1965.

[4 ] Bird, G.A., *Molecular Gas Dynamics*, Clarendon Press, Oxford, 1976.

[5 ] Dagum, L., *On the Suitability of the Connection Machine for Direct Particle Simulation*, Ph.D. Thesis, Dept. of Aeronautics and Astronautics, Stanford Univ., 1990.

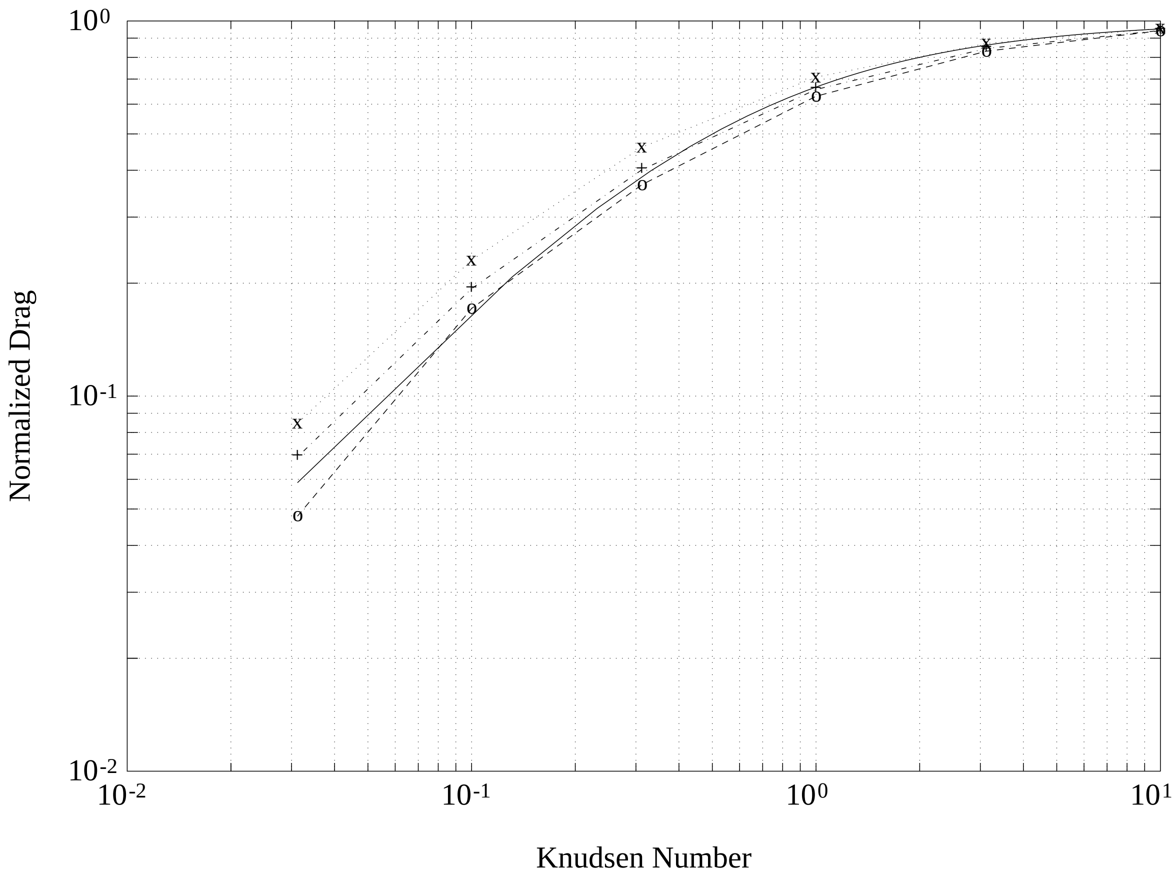


Figure 3: Normalized drag on moving surface in Couette flow as function of Knudsen number. Drag is normalized by the value in the free molecule limit. Results are presented for Maxwell (x), hard sphere (o), and inverse $9^{th}$ power law (+) interaction potentials. Lees' theoretical solution is given by the solid line.

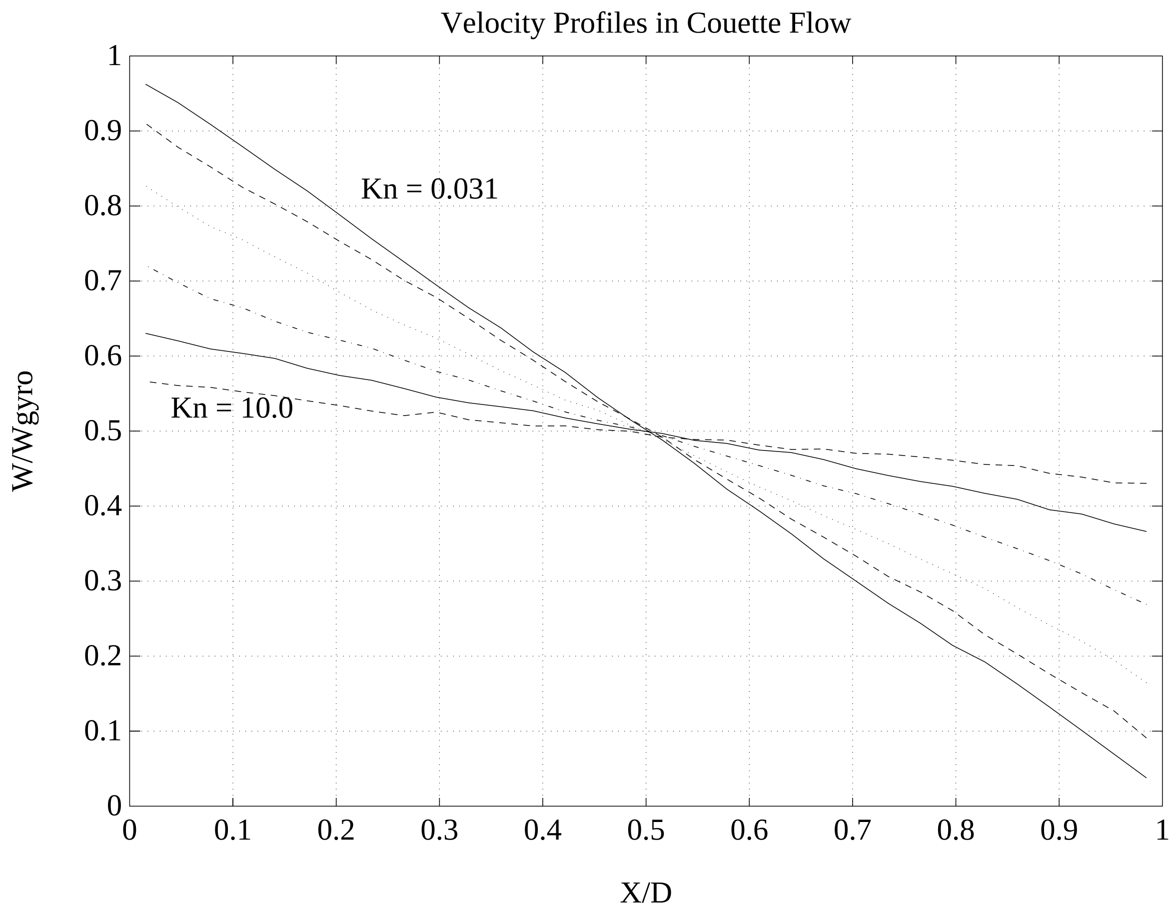


Figure 4: Velocity profiles as a function of Knudsen number for Couette flow with hard sphere interaction potential. Curves are: $K_n = 0.031$ —; $K_n = 0.10$ - - -; $K_n = 0.31$ ...; $K_n = 1.00$ -.-.-.; $K_n = 3.13$ —; $K_n = 10.0$ - - -.

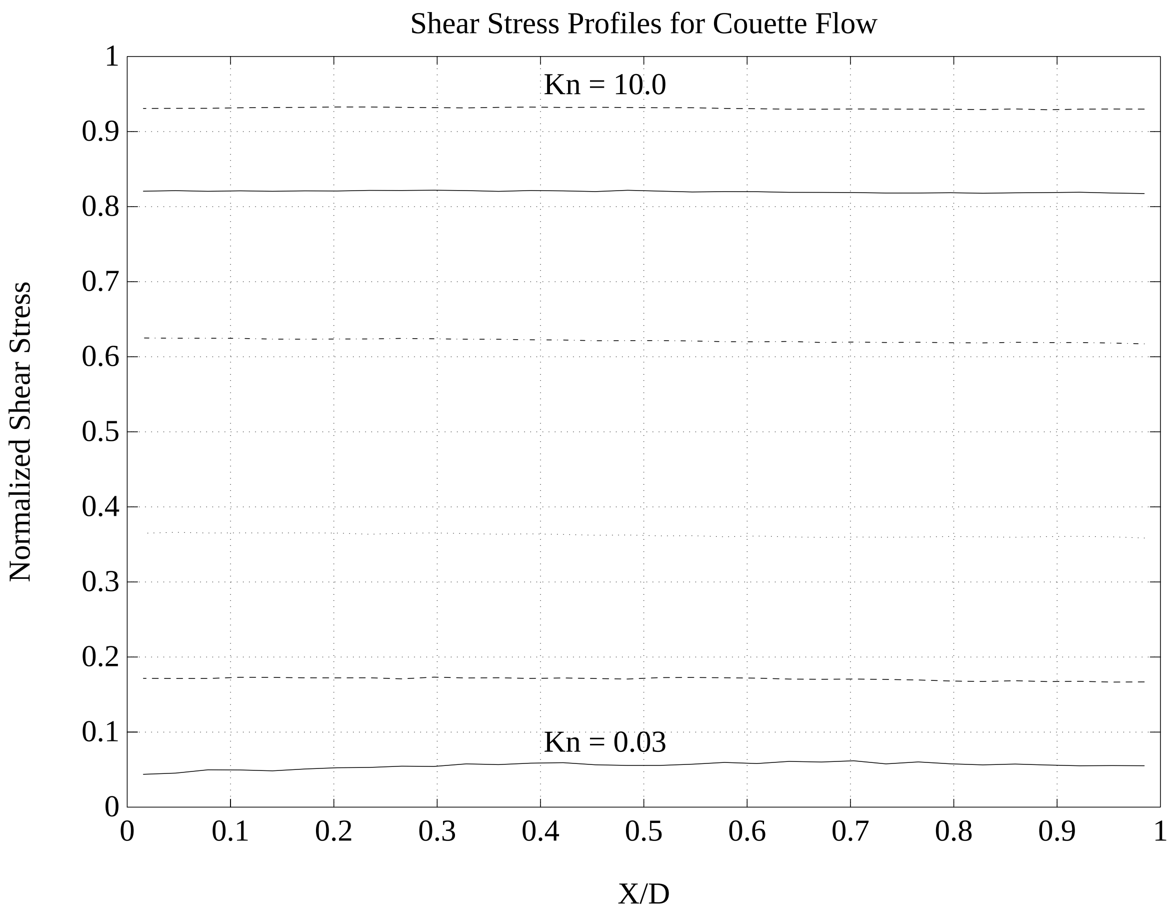


Figure 5: Couette shear stress profiles as a function of Knudsen number for a hard sphere interaction potential. Shear stress is normalized by the free molecule value. Position is normalized by the width between the moving and the stationary plate, $\delta$. Curves are: $K_n = 0.031$ —; $K_n = 0.10$ - - -; $K_n = 0.31$ ...; $K_n = 1.00$ -.-.-.; $K_n = 3.13$ —; $K_n = 10.0$ - - -.

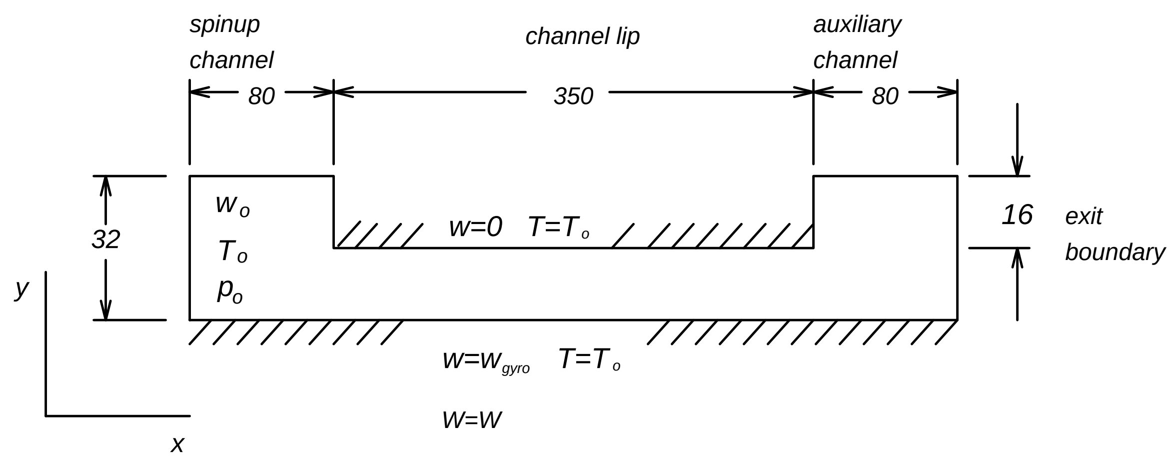


Figure 6: Geometry for Gravity Probe B simulation.

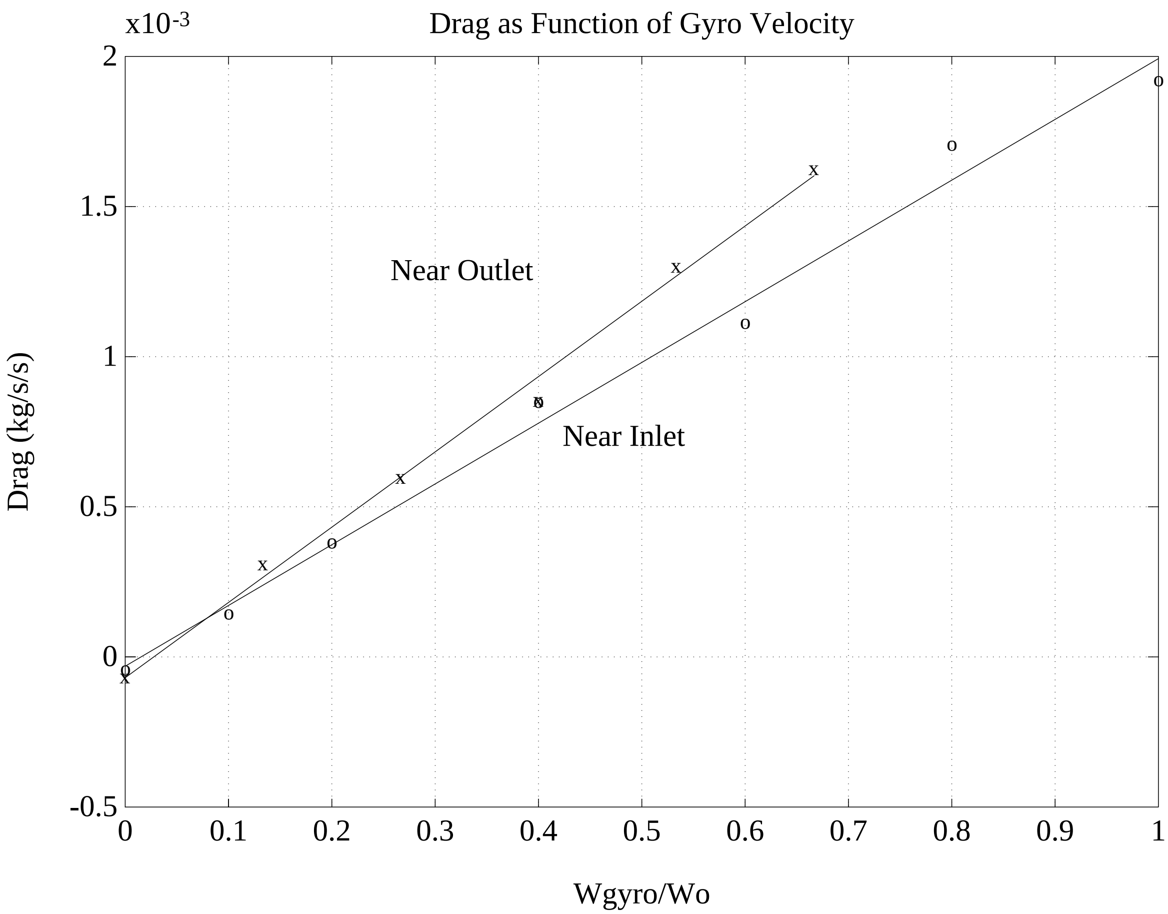


Figure 7: Lip leakage flow drag in Gravity Probe B simulation: 'o' Near Inlet; 'x' Near Outlet.

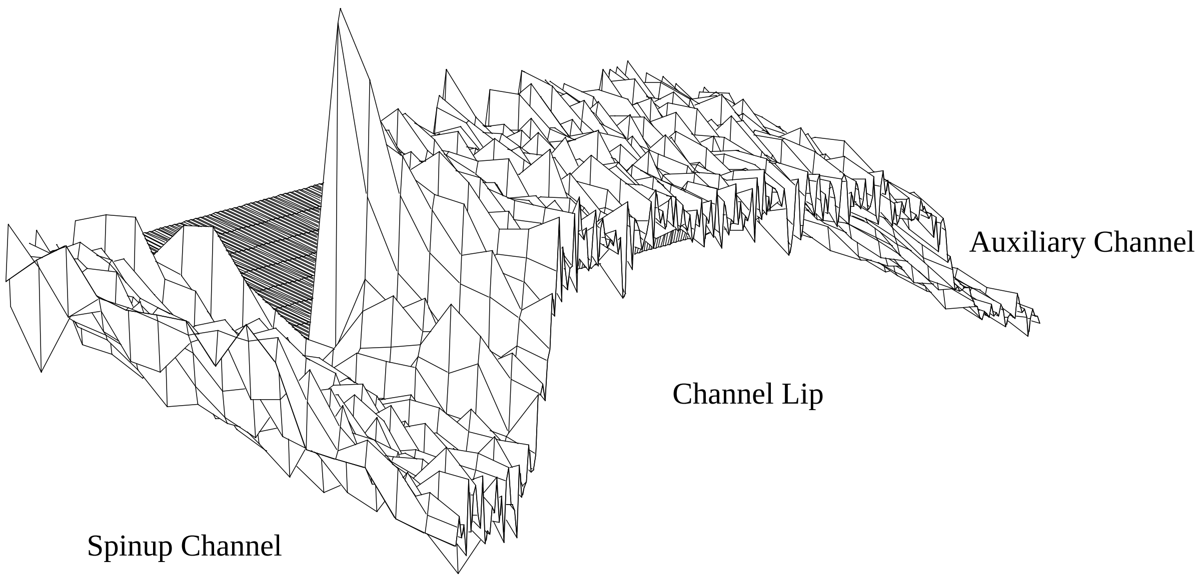


Figure 8: Shear stress in the lip leakage flow.

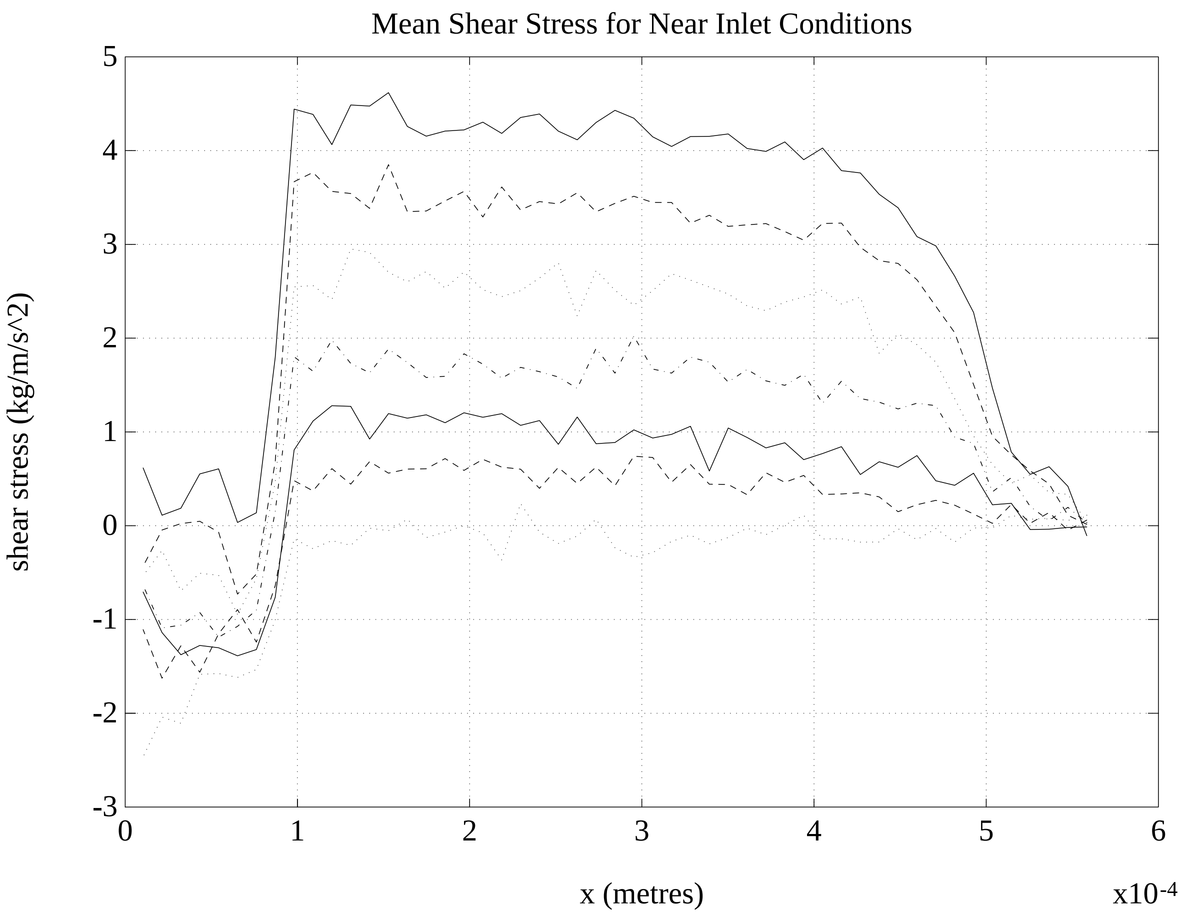


Figure 9: Shear stress through the channel lip section for near inlet conditions. Refer to table 1: run1 ....; run2 - - -; run3 —; run4 -.-.-.-; run5 ....; run6 - - -; run7 —.

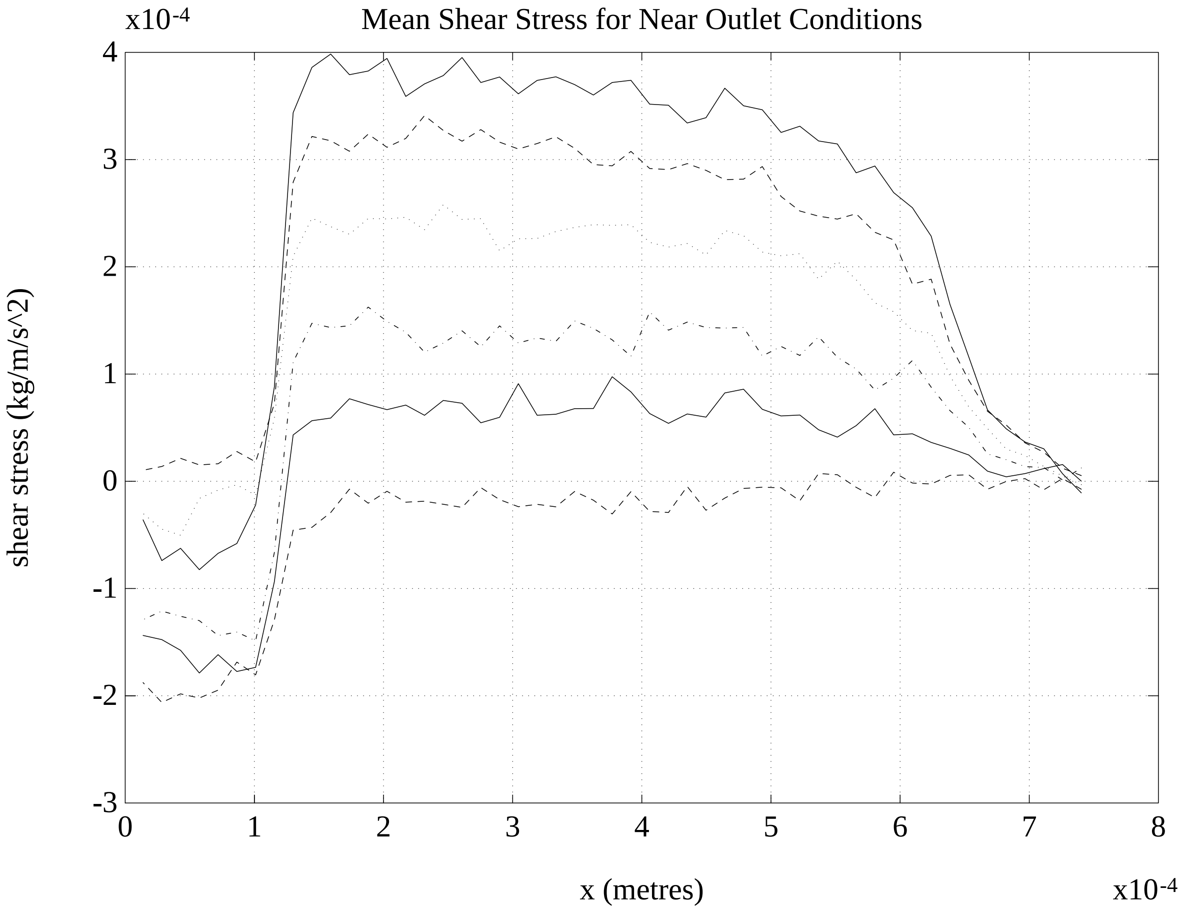


Figure 10: Shear stress through the channel lip section for near outlet conditions. Refer to table 2: run1 - - -; run2 —; run3 -.-.-.-; run4 ....; run5 - - -; run6 —.